Direct measurements of the Malvinas Current velocity structure

D.I. Frey[1], A.R. Piola[2], V.A. Krechik[1], D.V. Fofanov[1], E.G. Morozov[1], K.P. Silvestrova[1], R.Yu. Tarakanov[1], S.V. Gladyshev[1]

[1]Shirshov Institute of Oceanology, Russian Academy of Sciences, Moscow, Russia

[2] Departamento de Oceanografia, Servicio de Hidrografia Naval, CONICET, and Universidad de Buenos Aires, Buenos Aires, Argentina

Corresponding author: Dmitry Frey (dima.frey@gmail.com)

Key Points:

- Direct current observations across five Malvinas Current transects are presented.
- The new observations confirm a two-jet structure along the current path from northern Drake Passage to 46°S.
- In the upper 700 m the inshore and main current branches transport 2.4 – 6.3 Sv and 21.3 – 25.4 Sv, respectively.

Abstract

Direct velocity measurements of the Malvinas Current were carried out on multiple occupations of five transects across the flow using a Shipborne Acoustic Current Profiler (SADCP) on the R/V Akademik Sergey Vavilov and Akademik Mstislav Keldysh. These data are used to determine local features of the three-dimensional velocity field of the current. The occupations covered the northern branch of the Antarctic Circumpolar Current and the southern part of the Malvinas Current. Five transects across the flow were located at 350 – 550 km from each other from the Drake Passage to the western Argentine Basin at 46°S. The new observations reveal that the current is organized in two branches, namely, an inshore branch extending to a depth of 200-300 m and a main offshore branch, which flows approximately over the 1400 m isobath. This two-branch structure is observed on each of the cross-flow transects. The observed velocities of the inshore branch exceed 40 cm/s on each studied crossing of the current. The Malvinas Current is a cold western boundary current that follows the Subantarctic Front. This flow originates as an offshoot of the northern branch of the Antarctic Circumpolar Current and continues over the Falkland/Malvinas Plateau and along the western slope of the Argentine Basin. Volume transports of the upper 700 m of the Malvinas Current calculated for each crossing range between 1.4 – 4.4 Sv for the inshore branch and between 21.2 – 25.5 Sv for the offshore (main) branch.

Plain Language Summary

The Malvinas Current (MC) is one of the dominant circulation features in the Southwest Atlantic. It originates as the northern branch of the Antarctic Circumpolar Current (ACC) which is the largest ocean current in the global ocean. The ACC plays a significant role in the circulation in the Southern Ocean and our knowledge of its structure is important for understanding ocean dynamics and global climate changes. The ACC consists of three main circumpolar fronts from north to south: the Subantarctic Front (SAF), the Polar Front, and the southern ACC Front. The Malvinas Current is associated with the SAF over the Falkland/Malvinas Plateau and the continental slope of South America. Its spatial structure has been repeatedly studied based on ocean modeling, reanalysis data, satellite images, and measured distribution of temperature and salinity, but direct velocity measurements of the MC remain quite rare. In this work, we report unprecedented velocity measurements carried out across the current along five transects spanning

most of the current. These new data reveal that the current is organized in two branches in its southern part and allow us to calculate their volume transports and maximum speeds.

Introduction

The cold Malvinas Current (MC) is one of the main circulation patterns in the southwestern South Atlantic Ocean (Peterson & Whitworth III, 1989). This current originates as a branch of the Antarctic Circumpolar Current (ACC) (Provost et al., 1996), rounds east of the Falklands/Malvinas Islands, and flows northward along the continental slope of South America (Figure 1) (Wilson & Rees, 2000). The MC follows the Subantarctic Front (SAF), one of three main fronts of the ACC in the Drake Passage (Sokolov & Rintoul, 2009; Barre et al., 2011). It is generally accepted that the MC starts near the Burdwood Bank at around 55°S; upstream from the sharp northward turn of the SAF, the flow is referred to as the northern branch of the ACC (Artana et al., 2016). At approximately 38°S, the MC meets with the Brazil Current, generating a thermohaline front known as the Brazil Malvinas Confluence zone (Brennecke, 1921; Deacon, 1937). Further downstream, both currents retroflect and instabilities generate prominent mesoscale structures (Zyrjanov & Severov, 1979, Chelton et al., 1990). On average, the front intersects the 1000 m isobath at 38°30'S in summer and north of 37°S in winter (Artana et al., 2019a; Saraceno et al., 2004). Satellite-derived surface temperature, CTD, and ADCP observations showed that at 45°S the current consists of several fronts and jets (Franco et al., 2008; Piola et al., 2013). Two main branches, namely, the inshore and offshore jets are located approximately over the 200 m and 1400 m isobath, respectively; the flow is concentrated in these two relatively narrow (10-20 km) jets. It is suggested that these branches merge north of 42°S (Artana et al., 2018b). In the Scotia Sea, the inshore and main branches flow west and east of the Burdwood Bank, respectively (Piola & Matano, 2019). Further downstream the MC branches flow over the Falkland/Malvinas Plateau and subsequently along the western margin of the Argentine Basin. Altimeter observations indicate that the eddies originated in the abyssal plain reach the western slope of the Argentine Basin and frequently block the MC approximately at 48°S, thus modulating its volume transport (Artana et al., 2016).

The spatial structure of the Malvinas Current was studied based on ocean modeling and reanalysis data (Artana et al., 2018b; Fetter and Matano, 2008), satellite data (Magalhaes & Silva, 2017; Rudorff et al., 2014; Legeckis & Gordon, 1982; Wilson & Rees, 2000), and geostrophic calculations based on hydrographic data (Gordon & Greengrove, 1986). It was shown that the MC variability is linked with the variability of the ACC and this connection is masked by high-frequency oscillations (Fetter and Matano, 2008). The variability of the inshore branch velocity field is partially caused by the presence of trapped waves in the region (Poli et al., 2020). Internal waves with intense surface manifestations propagate in the opposite direction of the MC (Magalhaes & Silva, 2017). A study of the MC variability based on the analysis of 140 CTD-sections along 46°S revealed that the maximum transport is observed in April and September-October (Remeslo et al., 2004). As for direct velocity measurements, they were repeatedly performed in the Scotia Sea, mainly across the Drake Passage (Meredith et al., 2011). Total volume transports and variability of the ACC were calculated based on full-depth hydrographic and velocity observations (Cunningham et al., 2003; Firing et al., 2011; Renault et al., 2011) and a moored array (Donohue et al., 2016). Measurements performed by Shipborne Acoustic Current Profilers (SADCP) were used to study upper ocean currents, in particular, Ekman currents (Lenn and Chereskin, 2009; Rocha et al., 2016). Variability of the ACC in the northern Drake Passage was studied based on velocity measurements on 10 moorings (Ferrari et al., 2012). Velocity field and volume transports in the Drake Passage were also investigated based on the analysis of the GLORYS12 reanalysis and compared with direct velocity measurements (Artana et al., 2019b).

Unlike the Drake Passage and western Scotia Sea, direct velocity observations of the MC further downstream are quite rare. The first measurements were performed using floats at about 750 m depth, which resulted in velocity estimates of 30-40 cm/s (Davis et al., 1992). Detailed analysis of these data combined with the data from 100-m drogued surface drifters suggested that the flow presented a significant barotropic structure (Peterson et al., 1996). Underway and profiling acoustic doppler current profiler (ADCP) observations at 45-46°S indicate velocities in the MC core ranging between 45 and 60 cm/s at 200 m depth (Saunders and King, 1995; Painter et al., 2010; Piola et al., 2013; Morozov et al., 2016). Similar velocity measurements performed over the Falkland/Malvinas Plateau showed velocities up to 50 cm/s (Arhan et al., 2002), which is in good agreement with geostrophic calculations (Pérez-Hernández et al., 2017). The along-isobath geostrophic velocities low-passed filtered (20-day cutoff) derived from satellite altimetry are strongly correlated with the in-situ velocities collected near the northernmost extent of the MC (~ 40-41°S), with the dominant variability mode of the current strength associated with meridional fluctuations of the Subantarctic Front (Ferrari et al., 2017). Thus, the altimetry derived currents are a useful indicator of the spatial velocity distribution and their low-frequency variability.

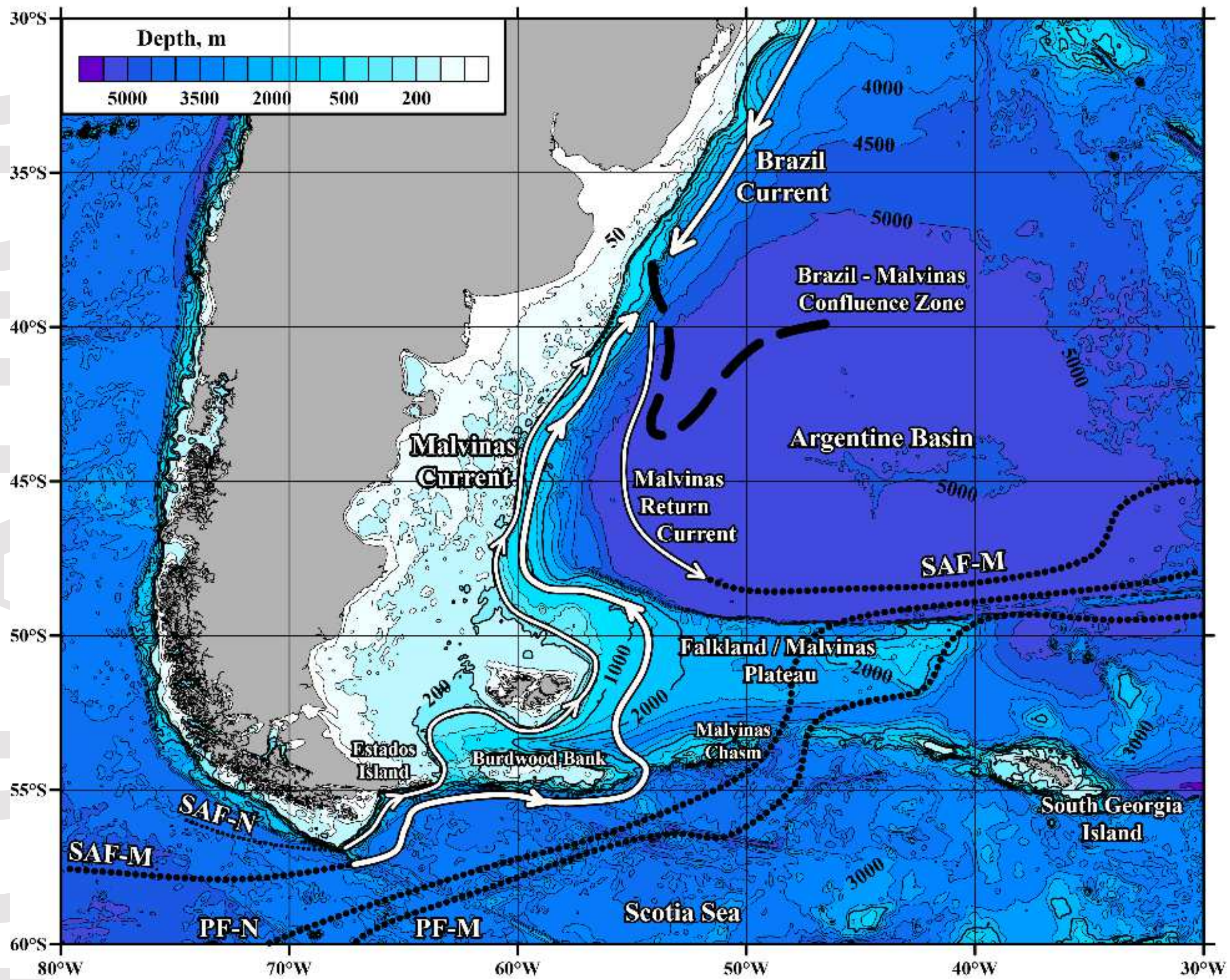

Figure 1. Mean surface circulation schematic in the western South Atlantic. Arrows indicate pathways of the main currents in the region; a thick dashed line indicates the mean location of the Brazil-Malvinas Confluence zone. Dotted lines are isolines of mean sea surface height corresponding to the ACC fronts: the northern branch of the Subantarctic Front (SAF-N, 23 cm), the main branch of the Subantarctic Front (SAF-M, -10 cm), the northern branch of the Polar Front (PF-N, -43 cm), the middle branch of the Polar Front (PF-M, -62 cm) according to (Barre et al., 2011; Artana et al., 2019b). The 200, 1000, and 2000 m isobaths are indicated by bold lines. The shoreline is shown according to the GSHHS data (Wessel, 1996), the bathymetry source is the GEBCO2019 database.

Previous studies report a wide range of transport estimates depending on the type of data, the season when the observations were collected, location, and depth of the measurements. The transport estimates range between 10 Sv (Gordon & Greengroove, 1986) and 70 Sv (Peterson et al., 1992). Vivier & Provost (1999a) estimated a mean MC transport of 41.5 ± 12 Sv based on the current meter measurements collected between 40° and 41°S from December 1993 to June 1995.

Detailed comparisons of different transport estimates are given in (Maamaatuaiahutapu et al., 1998) and (Piola et al., 2013). Recent calculations made on the basis of ADCP velocity measurements performed at 46°S give approximately 21 Sv in the upper 600-meter layer and 31 Sv from the surface to the bottom (Morozov et al., 2016), while combined satellite altimetry and in-situ observations collected near 41°S lead to a 24-year mean transport of 37.1 ± 2.6 Sv (Artana et al., 2018a). These latter MC transport estimates present strong variability at 30–110 days, semiannual, and annual periods.

In this work, we focus on the study of the MC structure along its path from the origin at the northern branch of the ACC in the Drake Passage and up to 46°S, upstream from the Brazil-Malvinas Confluence. We use shipboard ADCP (SADCP) velocity data collected over multiple crossings of five cross-current transects occupied along the current path. We also use data from satellite altimetry to investigate the spatial structure of the current at the time of the in-situ measurements. Using these data, we study the kinematic properties of the MC and calculate its volume transports at different locations. The goal of our research is to summarize our direct measurements and analyze the results comparing them with the remote data and previous studies.

2. Data and methods

This study is focused on the three-dimensional structure of the MC based on direct velocity measurements at different locations. The vertical structure of the horizontal velocity was observed along five cross-current transects occupied along the path of the northern ACC and MC using a SADCP system. Measurements were repeated several times between December 2016 and February 2020 (see Table 1 for details). We use satellite altimetry data to provide a regional view of the circulation and a qualitative understanding of how observed currents differ from the mean circulation pattern along the transect lines.

The general description of the transects is provided in section 2.1; the equipment and processing techniques are described in detail in section 2.2; the satellite altimetry data used to determine the time averaged circulation and the spatial structure at the time of each in-situ survey are discussed in section 2.3.

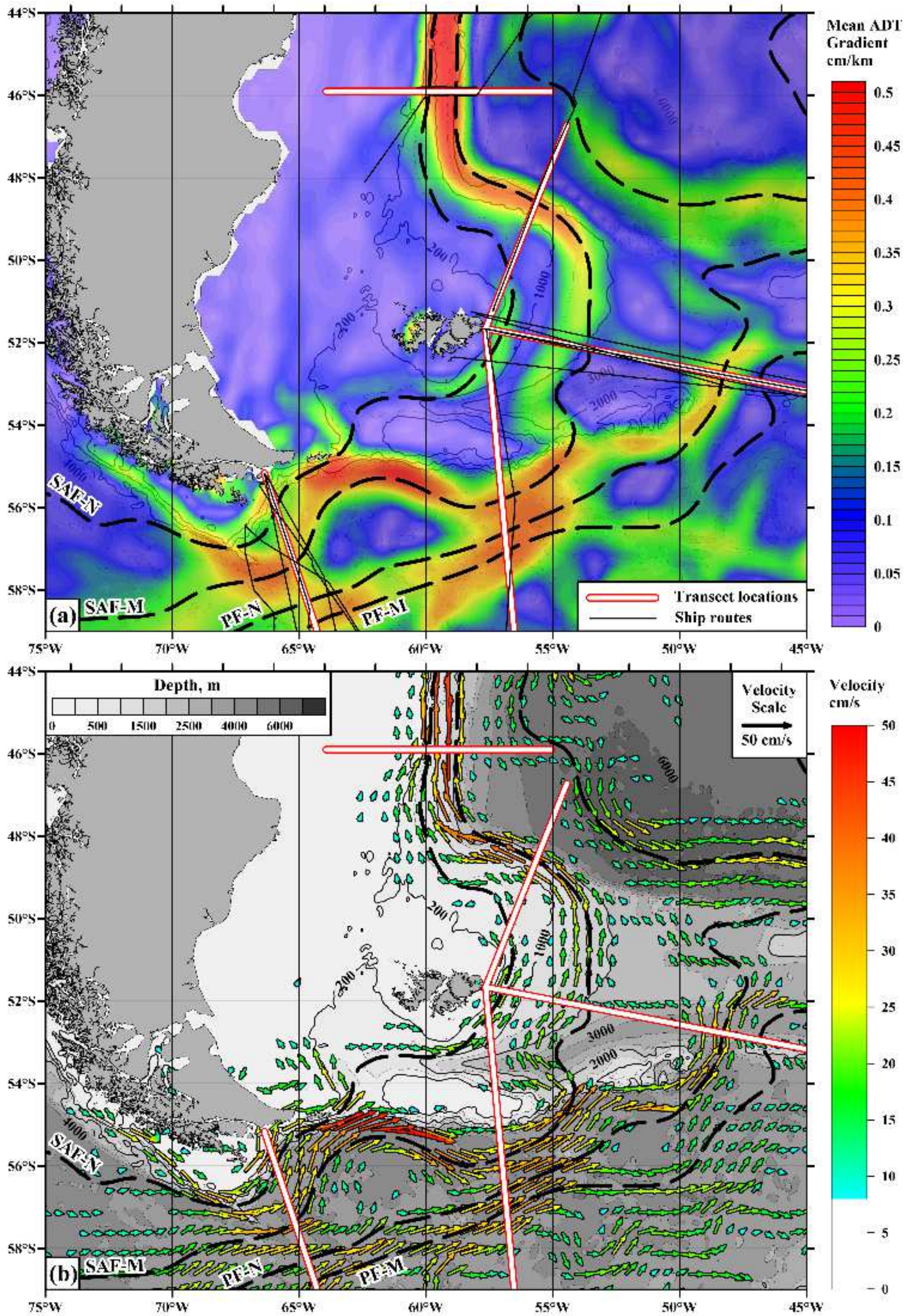

Figure 2. Gradient (cm/km) of the mean ADT averaged over 26-year period (a) and mean current velocities derived from these data (b). Arrows are shown only for mean velocities exceeding 8 cm/s. Locations of the SADCP Transects (1-5, see Table 1) used in this work are shown with red lines; ship tracks are shown with thin black lines in panel (a). The 200, 1000, and 2000 m isobaths are indicated by bold lines. The mean locations of the SAF-N, SAF-M, PF-N, and PF-M fronts are shown with dashed lines.

2.1. Transects across the current

Locations of the transects have been selected according to the satellite altimetry data in five regions across the flow in the northern Scotia Sea, over the Falkland/Malvinas Plateau, and in the Argentine Basin (Figure 2). Gradients of the mean Absolute Dynamic Topography (ADT) (Figure 2a) and calculated geostrophic velocities (Figure 2b) show that the transects are approximately perpendicular to the mean flow direction. Ship tracks are also shown in Figure 2a; more detailed information about the in-situ observations is presented in Table 1. Due to rough weather conditions, we slightly changed the routes of transects 1 and 2 in the western Scotia Sea (Figure 2a). To analyze the MC cross-flow structure, we projected the velocity to the direction perpendicular to each transect line, hereafter referred to as along-slope current. We checked the real direction of the MC branches using measured SADCP velocities and satellite altimetry data; the difference between these estimates of the MC direction and the along-slope component usually does not exceed 20-30°. We present all values of the MC direction for each of our 16 crossings in Supporting Information (Table S1) together with other parameters including maximum velocities, location of the velocity maxima, and transports of the MC branches.

Some of the transects shown in Figure 2 were occupied several times; the actual routes along each transect slightly differ from each other but generally they are located close to each nominal line. Typical distances between the real and nominal lines are about 20-30 km reaching a maximum distance of 100 km at one remote point of Transect 4 (Table 1). Transect 1 is located in the northern Drake Passage; Transects 2, 3, and 4 started around the western part of the Falkland/Malvinas Plateau are directed approximately southward, eastward, and northward, respectively; while Transect 5 is zonally oriented along 46°S. The distance between the transects along the current path varies from 350 (Transects 3 and 4) to 550 km (Transects 1 and 2).

Table 1. Crossings of the MC with SADCP measurements analyzed in this work. Abbreviations of the cruises are: ASV43 – 43^{rd} cruise of the R/V "Akademik Sergey Vavilov", October – November 2016; ASV45 – 45^{th} cruise, October 2017 – January 2018; ASV46 – 46^{th} cruise, October – November 2018; ASV47 – 47^{th} cruise, November – December 2018; AMK79 – 79^{th} cruise of the R/V "Akademik Mstislav Keldysh", December 2019 – February 2020. More details are given in the text.

Transect number (Figure. 2)	Crossing number	Cruise	Date (d.m.yr) and time (GMT)		Coordinates		Transect orientation (° true)
			Start	End	Start	End	
1	1	ASV45	01.12.2017	04.12.2017	63°56.44 S	55°10.67 S	074

			18:50	01:40	60°49.54 W	66°21.32 W	
	2	ASV45	05.12.2017 04:24	07.12.2017 04:24	55°09.60 S 66°23.69 W	64°29.72 S 63°04.89 W	074
	3	ASV45	11.01.2018 21:12	14.01.2018 08:17	62°31.74 S 59°23.85 W	55°22.86 S 66°35.23 W	074
	4	AMK79	16.01.2020 10:59	19.01.2020 11:41	55°15.47 S 65°31.80 W	63°08.42 S 63°05.98 W	074
	5	AMK79	04.02.2020 10:52	06.02.2020 10:22	61°24.39 S 60°06.46 W	56°25.83 S 67°07.99 W	074
	6	AMK79	10.02.2020 03:06	12.02.2020 10:58	55°13.57 S 66°17.44 W	62°43.81 S 62°05.07 W	074
2	7	ASV45	31.12.2017 00:07	02.01.2018 11:25	51°40.23 S 57°38.10 W	62°05.54 S 57°58.08 W	085
3	8	ASV45	21.10.2017 21:50	25.10.2017 14:16	51°40.26 S 57°49.49 W	54°09.30 S 37°30.51 W	101
	9	ASV45	29.10.2017 22:25	02.11.2017 00:59	53°55.64 S 38°07.67 W	51°18.70 S 58°00.28 W	101
	10	ASV45	05.11.2017 00:18	07.11.2017 17:41	51°39.58 S 57°40.94 W	54°10.89 S 37°31.78 W	101
	11	ASV45	13.11.2017 02:16	16.11.2017 09:25	53°54.19 S 37°31.66 W	52°24.79 S 59°21.96 W	101
	12	ASV45	18.11.2017 22:19	21.11.2017 11:24	51°39.82 S 57°38.18 W	53°55.61 S 37°46.52 W	101
	13	ASV45	25.12.2017 14:01	28.12.2017 18:06	53°56.45 S 37°27.48 W	51°14.79 S 58°13.71 W	101
4	14	ASV45	16.10.2017 13:25	21.10.2017 00:53	39°24.36 S 50°41.68 W	51°04.60 S 57°18.11 W	023
5	15	ASV43	12.11.2016 10:47	13.11.2016 00:39	46°00.00 S 58°00.10 W	45°59.93 S 59°45.23 W	090
	16	AMK79	12.01.2020 16:01	13.01.2020 05:32	45°47.95 S 58°00.13 W	45°48.32 S 60°21.34 W	090

2.2. Direct velocity observations

The underway SADCP data were collected by two research vessels, “Akademik Sergey Vavilov” and “Akademik Mstislav Keldysh” (Table 1) equipped with identical SADCP systems – Teledyne RD Instruments Ocean Surveyor (TRDI OS) SADCP with a frequency of 76.8 kHz. Some peculiarities of SADCP measurements in the Southern Ocean are listed in (Firing et al., 2012). During all our surveys the profilers were set in the narrowband mode, which increases the profiling range up to 700 meters depth. We set from 60 to 100 vertical bins 16 or 8 meters each with an 8-meter blank distance immediately below the transducer. The draught of the ship is 6 m, which gives 22 or 18 m depth for the center of the first bin (the depth of the uppermost layer with velocity measurements). Time averaging of the raw data was made over 120 s intervals. Since the ship speed varied between 8 and 10 knots, this time average represents an along-track averaging of roughly 500 m. The SADCP data were smoothed with a horizontal scale of 25 km, which is approximately equal to the resolution of the altimetry data; we estimated the maximum velocity of the MC branches based on these data. The maximum velocity jets were defined as bands within the current speed higher than 90% of the maximum velocity value. Measurement errors in the amplitude of the horizontal velocities were small, approximately 1–2 cm/s (Chereskin and Harris, 1997). We multiply the maximum velocity error (2 cm/s) by the current cross-section for calculations of the volume transport error bars. Some additional errors can be caused by non-simultaneity of SADCP measurements (Tarakanov, 2018). The TPXO9 model (Egbert & Erofeeva, 2002) was used to subtract the barotropic tidal velocities at the moment of measurements. Typical tidal velocities in the region of our transects are insignificant in the open ocean (usually less than 2-3 cm/s) and higher near the continental shelf (up to 10-15 cm/s). Thus, tides can significantly affect the flow structure of the inshore branch.

2.3. Satellite altimetry data

We used a satellite altimetry gridded product (Pujol et al., 2016) available from Copernicus Marine Environment Monitoring Service (CMEMS, http://marine.copernicus.eu/). These data have a spatial resolution of 0.25° and a daily temporal resolution. The product includes data from all available altimeters at any given time. We used different types of altimetric data: Absolute Dynamic Topography (ADT), Sea Level Anomalies (SLA), and zonal and meridional components of computed surface geostrophic velocities. It is known that these geostrophic velocities are strongly correlated with the in-situ velocity observations collected in the MC at 41°S (Ferrari et al., 2017); in this work, we compare these velocities at different locations of the MC. Average surface-geostrophic velocities were also used for the analysis of the mean regional circulation (Figure 2b). Satellite data have advantages and limitations; in general, satellite-derived velocities have a smaller amplitude than the in-situ velocities, as well as a lower standard deviation (Ferrari et al., 2012). Though gridded altimetry data are provided with a daily resolution, the satellite revisit time is about 9.9 days or longer, depending on the platform. Thus, altimetry derived products do not capture velocity fluctuations typically shorter than about 20 days. Consequently, satellite derived geostrophic velocity is significantly correlated with in-situ observations only after the data are 20-day low-pass filtered (e.g., Ferrari et al., 2017). Altimetric mapping tends to smooth the fronts and reduce the velocities of the associated currents. Despite the previously mentioned limitations, the use of altimetry data allows us to study ocean circulation with regular temporal and spatial resolution, which provides a context for the results of single transects both in time and space.

3. Spatial structure of the MC

We analyze the spatial structure of the MC and northern branch of the ACC at five transects across the flow; their locations are shown in Figure 2. The analysis of these data is presented for three different regions, namely, the Scotia Sea, the Falkland/Malvinas Plateau, and the Argentine Basin south of 46ºS. The results for these three regions are presented below.

3.1. Structure of the current in the Scotia Sea

We made measurements at two different quasi-meridional sections across the current in the western Scotia Sea: along Transect 1 in the Drake Passage and along Transect 2 south of the Falkland/Malvinas Islands. Here, we focus on the northern segments of these two transects. Synoptic altimetry-derived sea surface velocity maps for these two crossings at the time of in situ measurements are shown in Figure 3a for Transect 1 and in Figure 3b for Transect 2.

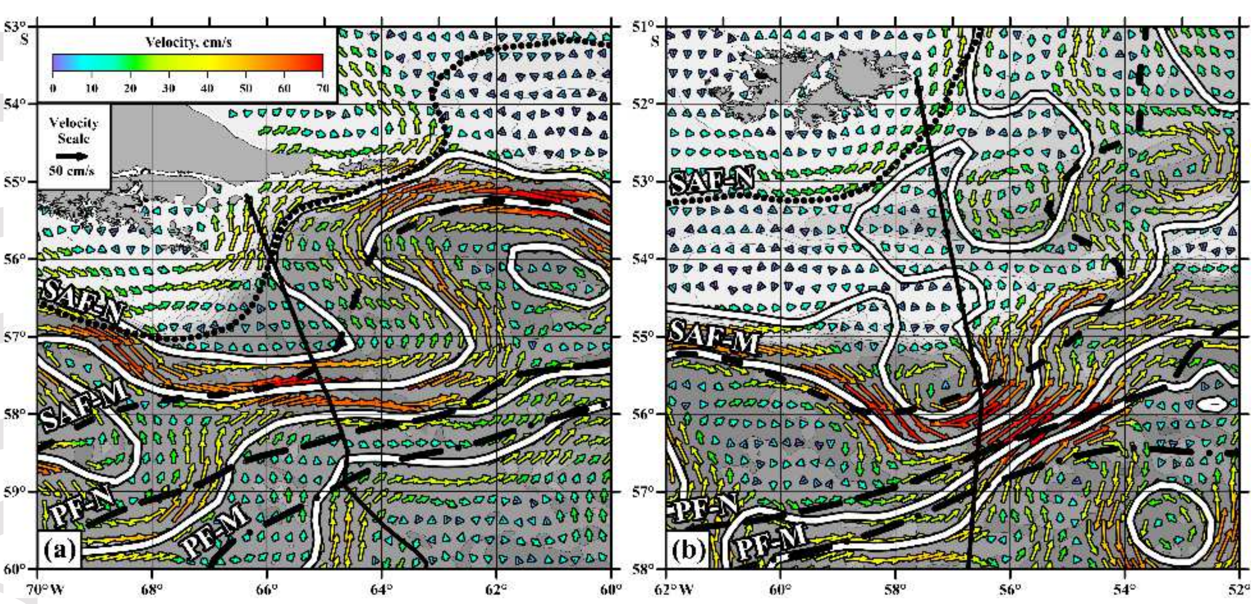

Figure 3. Altimetry-derived sea surface geostrophic circulation in the Scotia Sea on December 2, 2017 (a) and December 31, 2017 (b). The dates correspond to crossings 1 and 7 (see Table 1 for additional information). Black lines denote ship routes along Transect 1 (a) and 2 (b); white lines are synoptic locations of the SAF-N, SAF-M, PF-N, and PF-M fronts. Mean locations of the fronts are shown with dotted (SAF-N), dashed (SAF-M), long-dashed (PF-N), and dashed-dotted (PF-M) lines.

The results of SADCP measurements in the northern part of these sections are presented in Figures 4 (Transect 1 in the Drake Passage) and 5 (Transect 2 south of the Falkland/Malvinas Islands). The northern branch of the ACC, which feeds the MC, is not located near the continental slope of South America; instead, it flows eastward at a distance of 200 km from the shelf break. The mean position of the northernmost ACC branch is located further north and closer to the South America shore than at the time of measurements along Transect 1. The more frequent location of the main northern branch of the ACC is about 100 km from the shore (see Supplementary Figures). The mean locations of the Subantarctic Front and northern and middle branches of the Polar Front are shown in Figure 3 according to (Kim & Orsi, 2014; Barre et al., 2011). On occasions, these meandering fronts may come close to each other or merge completely. For example, the intense jet observed on Transect 1 in the Drake Passage in early December 2017 (Figure 4) is associated with a southward deflection of the SAF-N and a northward deflection of the PF-N (Figure 3a). Similar frontal displacements are also apparent near Transect 2 in late December 2017 (Figure 3b and 5). In other cases, these fronts are clearly separated (Figure S2, S3). When there are multiple intersections between Transect 1 and SAF-N we reported the northernmost crossing. An additional shallow current branch is observed along the upper continental slope (Figure 3); its vertical extent reaches about 200 m and the velocities exceed 50 cm/s (Figure 4). This inshore branch flows in the northward direction closely aligned with the orientation of the upper continental slope, unlike the main branch, which flows nearly eastward (Figure 3a and 4c). The mean vertical shear of the inshore branch estimated in the upper 200-meter layer reaches $3*10^{-3}$ s^{-1} in the center of the jet. The shear of the main branch estimated in the upper 700 m is much lower and equals $1*10^{-3}$ s^{-1}. The inshore branch is observed over all sections occupied in the northern ACC and the MC. The SADCP observations also reveal a flow in the opposite direction located between the inshore and main branches. Its width is about 150 km and velocities reach 25 cm/s between the sea surface and 200 m depth at a distance of 200 km from the shore (Figure 4e). Inspection of the altimetry derived velocity field suggests that the reversing flow across Transect 1 is associated with the strong anticyclonic meander of the northern branch of the ACC downstream of the transect (Figure 3a). These bands of opposite flow are observed on most crossings of the current (Figures 4, 5, S1-S5) and are apparent both in the SADCP data and altimetry-derived sea surface geostrophic velocities.

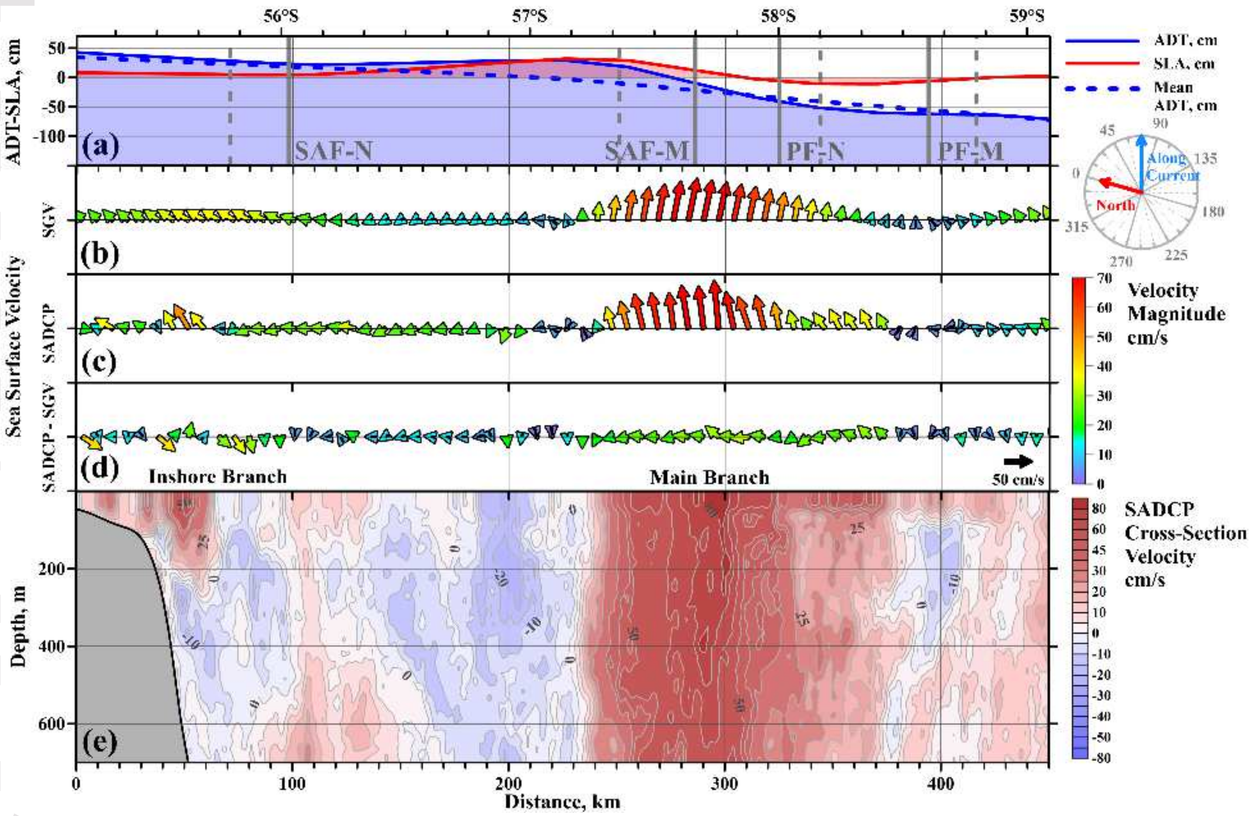

Figure 4. Transect 1, occupied in the northern Drake Passage on December 1-4, 2017 (Crossing 1; see Table 1 and Figure 2 for location). Top panel (a): altimetry data at the time of measurements: Absolute Dynamic Topography (ADT, solid blue line), Sea Level Anomaly (SLA, solid red line), and time mean ADT (dashed blue line). Panel (b): satellite-derived sea surface geostrophic velocities (SGV) along the SADCP transect. Panel (c): sea surface velocities based on the SADCP data. Panel (d): difference between measured and altimetry-derived velocities. The true north and along-slope directions are shown to the right of panels (a) and (b). Bottom panel (e): along-slope SADCP velocities across the northern ACC branch. The mean locations of the SAF-N, SAF-M, PF-N, and PF-M fronts are shown with dashed gray lines based on the isolines of mean sea surface height of 23 cm, -10 cm, -43 cm, and -62 cm according to (Barre et al., 2011). The synoptic location of the same isolines is shown with vertical solid gray lines. Minor ticks along the x-axis denote 10 km spacing hereafter.

The Burdwood Bank separates the inshore and main branches, which is seen over Transect 2 (Figure 5). This crossing is located just downstream of an anticyclonic eddy (Figure 3b) which explains the northeastward velocity component at a distance of 400 km from the shore (Figure 5b and c). The main MC branch is characterized by an intense velocity core reaching 75 cm/s at 250 m, and lower sea surface velocity (maximum ~ 58 cm/s). Altimetry-derived and SADCP velocities are in good agreement (the maximum difference is about 20 cm/s for the intense main branch). The maximum velocities of the inshore branch are 42 cm/s and directed to the northeast based on direct measurements; while the amplitudes of altimetry-derived SGV are smaller, reaching 24 cm/s.

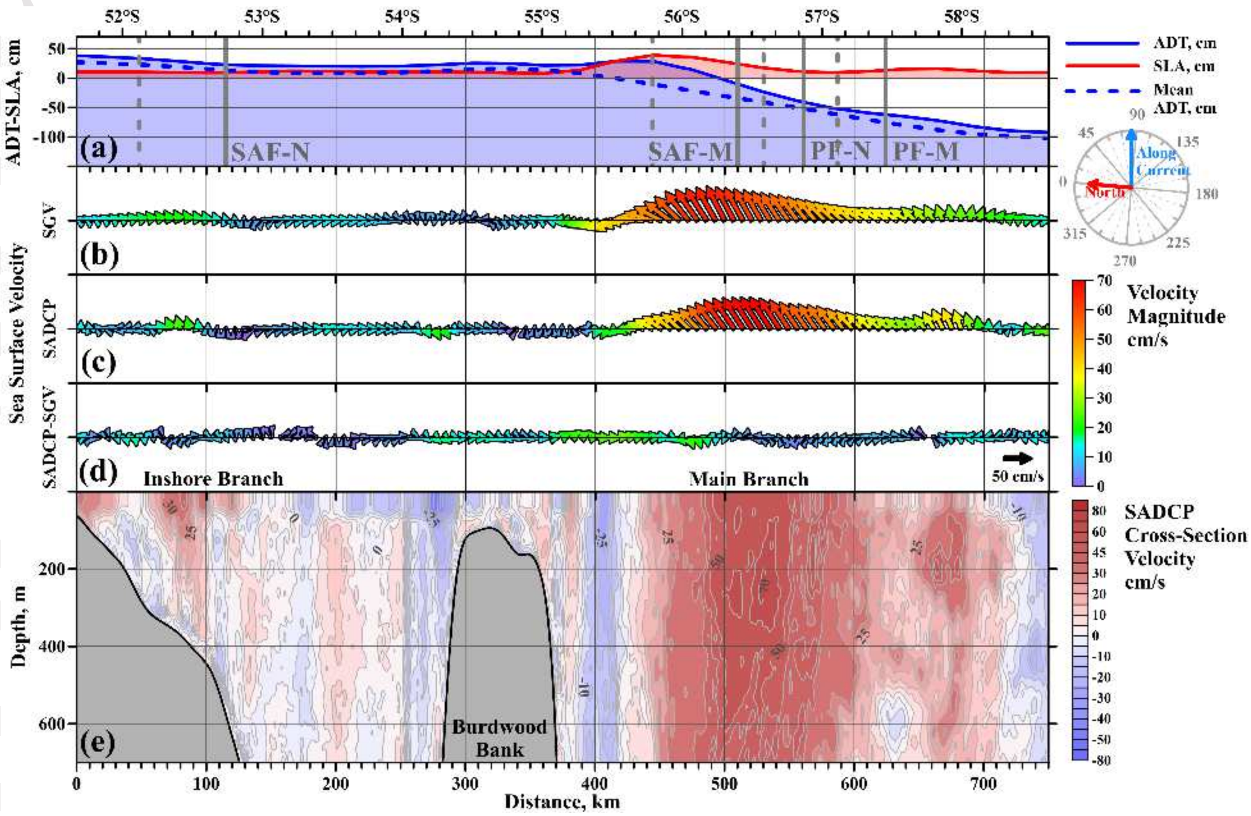

Figure 5. Transect 2, occupied in the Scotia Sea on December 31, 2017 – January 02, 2018 (Crossing 7; see Table 1 and Figure 2 for location). Top panel (a): altimetry data at the time of measurements: Absolute Dynamic Topography (ADT, solid blue line), Sea Level Anomaly (SLA, solid red line), and time mean ADT (dashed blue line). Panel (b): satellite-derived sea surface geostrophic velocities (SGV) along the SADCP transect. Panel (c): sea surface velocities based on the SADCP data. Panel (d): difference between measured and altimetry-derived velocities. The true north and along-slope directions are shown to the right of panels (a) and (b). Bottom panel (e): along-slope SADCP velocities across the northern ACC branch. The mean locations of the SAF-N, SAF-M, PF-N, and PF-M fronts are shown with dashed gray lines based on the isolines of mean sea surface height of 23 cm, -10 cm, -43 cm, and -62 cm according to (Barre et al., 2011). The synoptic location of the same isolines is shown with vertical solid gray lines.

The complex structure of the northern ACC branch in the Scotia Sea south of the Falkland/Malvinas Plateau is revealed from time-averaged satellite altimetry derived circulation (Figure 6). East of Tierra del Fuego the inshore and main branches diverge sharply following the bottom topography. The inshore branch that flows along the 200 – 300 m isobaths veers northward through the passage between Estados Island and the Burdwood Bank and continues along the upper continental slope around the Falkland/Malvinas Islands. This passage is relatively shallow (< 600 m) and prevents the flow of the main MC branch. Thus, the main branch flows along the southern slope of the Burdwood Bank, closely following the 1400 isobath; then part of this flow rounds the eastern slope of the Burdwood Bank and the Malvinas Chasm; and finally turns northward and flows along the western slope of the Falkland/Malvinas Plateau. A significant fraction of the main branch continues eastward as part of the ACC. The distance between the main and inshore branches of the MC along Transect 2 reaches 400 km (Figure 5). Approximately at 53°S, both branches merge and continue flowing northward alongside at a distance about 100 km between each other. All these features of the MC can be clearly seen in the mean velocity field derived from the mean dynamic topography (Figure 6), the SADCP observations (Figure 5, see also Artana et al., 2018b), hydrographic data (Piola and Gordon, 1989), and numerical simulations (Fetter and Matano, 2008; Combes and Matano, 2018; Guihou et al., 2020). Based on these observations we suggest that the inshore branch of the MC originates east of Estados Island, while the main branch originates east of the Burdwood Bank.

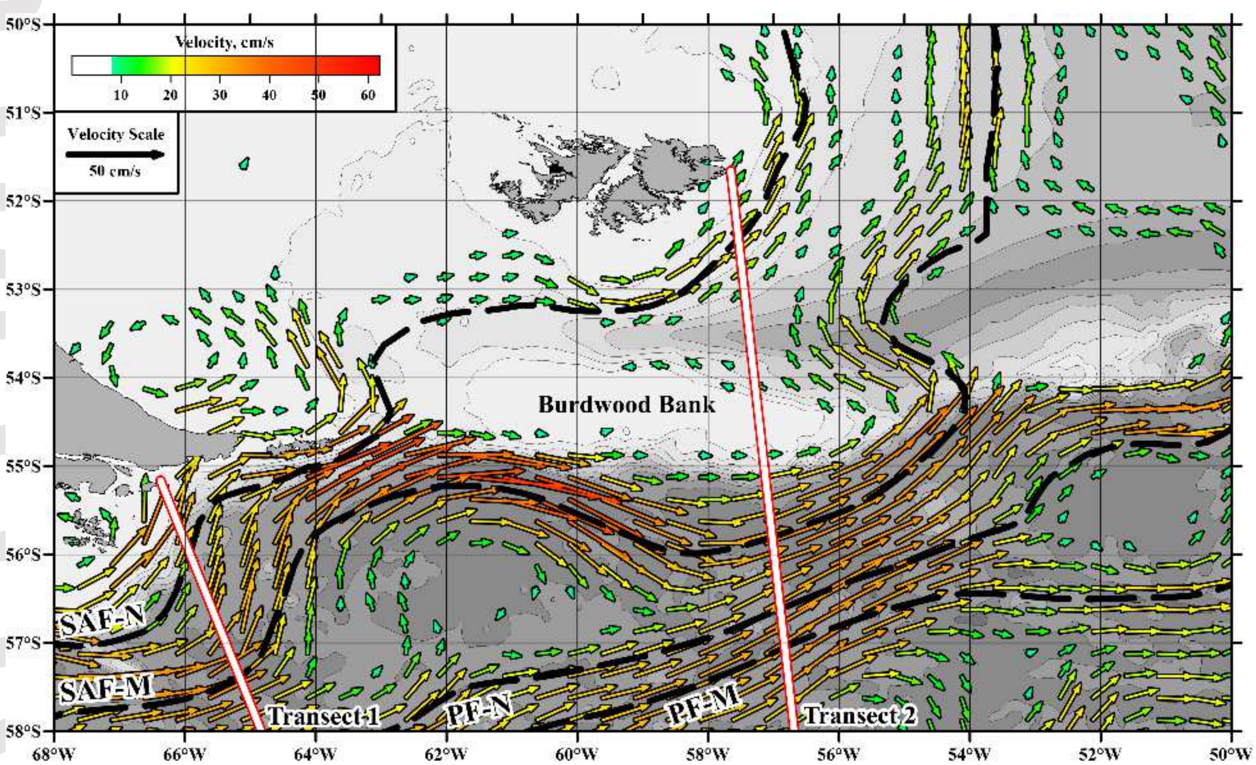

Figure 6. Inshore and main (offshore) branches of the MC in the northern Drake Passage and western Scotia Sea. Time-averaged over 26 years geostrophic velocities derived from the mean

satellite altimetry data are shown with colored arrows. Only velocities higher than 8 cm/s are shown; the magnitudes of the current speeds are shown with both colors and vector length. Locations of the fronts are shown with dashed black lines.

3.2. The flow over the Falkland/Malvinas Plateau

The altimetry derived circulation and frontal locations during each of the six occupations of transect 3 are presented in Figure 7. The locations of the SAF-N and SAF-M, and the associated high velocity cores in this region are quite variable, presenting meanders and eddies. This observation is in agreement with the moderate increase in altimetry and model derived eddy kinetic energy (300-400 cm^2/s^2) observed downstream of the Malvinas Chasm (e.g., Artana et al., 2016, 2018c). Figure 8 presents the SADCP section occupied 21-25 October 2017, together with the altimetry derived ADT, SLA and SGV sections. At this time the SAF-N runs nearly parallel to the section (Figure 7a) but the inner MC core is located close to the climatological location of the front (Figure 8e). The main core of the MC as depicted by both, the SADCP and altimetry surface geostrophic velocity, is located west of the SAF-M (Figure 8a and 8e). This indicates that at this time the SAF-M is associated with higher ADT values than those defined by Barre et al. (2011). Similar discrepancies are observed at the SAF-N front (Figure 7) and this is possibly due to spatial and temporal variations of the ADT value corresponding to the front location. Specific time-averaged ADT values that match SAF-N and SAF-M fronts in the northern Drake Passage do not necessarily match so well further downstream. In addition, there are time variations of the ADT associated with the highest ADT gradients at each location. All other crossings along Transect 3 are presented in Supporting Information for this article (Figures S6 to S10). In both branches, the maximum velocities are observed at the sea surface; the maximum of the inshore branch (60 cm/s) is located over the 200-m isobath; and that of the main branch (43 cm/s) is over the 1500-m isobath. The widths of the maximum velocity cores, defined as bands where the current speed exceeds 90% of the maximum, are 4.3 and 18.6 km for the inshore and main MC branches, respectively. Horizontal scales of the current width are 50 km for the inshore branch and 150 km for the main branch. Mean sea surface velocities within these limits are 26 cm/s and 21 cm/s for the inshore and main MC branches, respectively. The mean vertical shears of the inshore and main branches are $2*10^{-3}$ s^{-1} and $4*10^{-4}$ s^{-1}, respectively. Additionally, less intense and shallower high-velocity filaments are apparent east of the inshore branch. These less intense features are also observed in all other occupations of Transect 3 (Figure 9 and Supplementary Material, Figures S6 to S10).

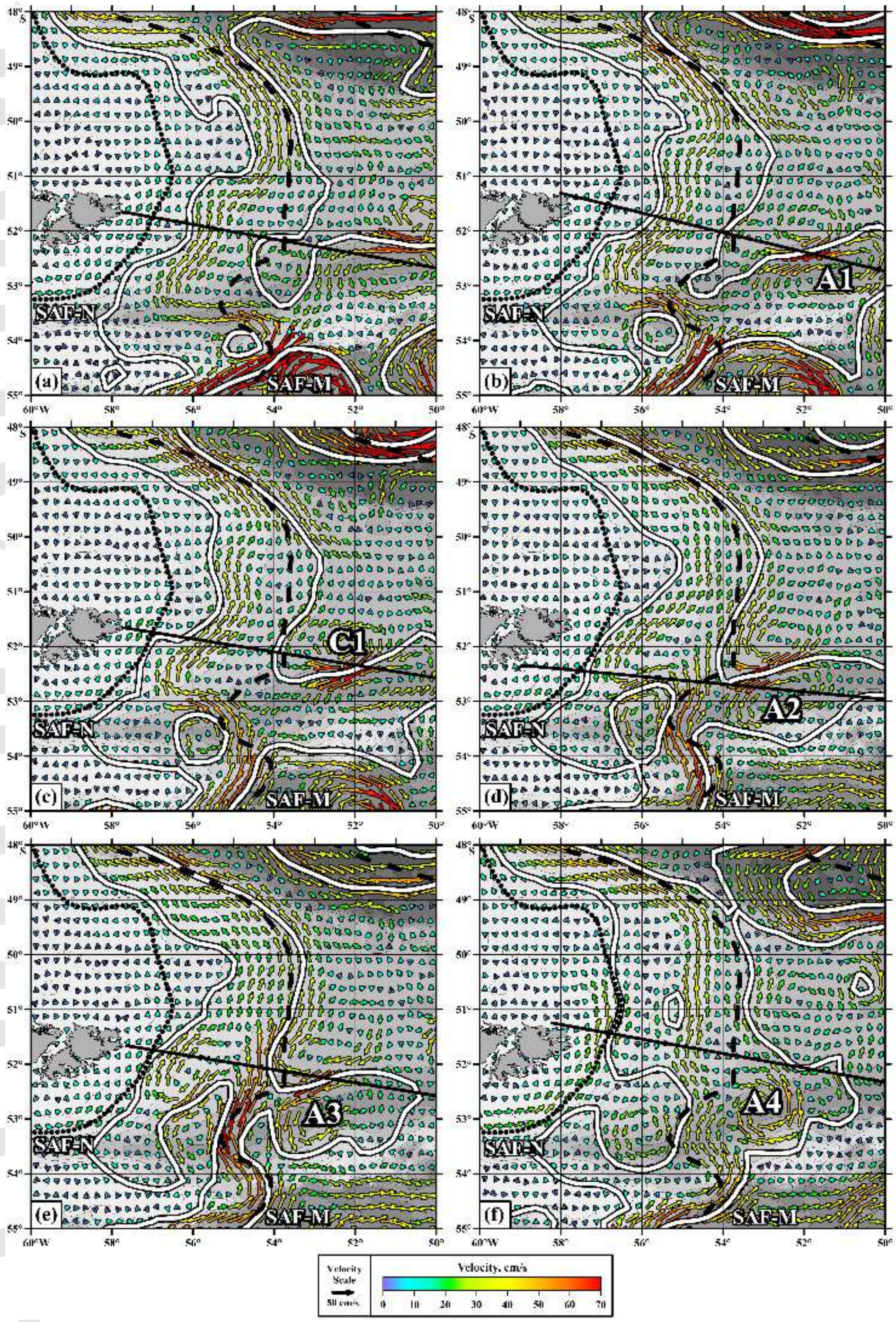

Figure 7. Altimetry-derived sea surface geostrophic circulation over the Falkland/Malvinas Plateau on October 22, 2017 (a), November 01, 2017 (b), November 05, 2017 (c), November 15, 2017 (d), November 19, 2017 (e), December 25, 2017 (f). The dates correspond to crossings 8, 9, 10, 11, 12, and 13 (see Table 1 for additional information). Black solid lines denote ship routes; white lines are synoptic locations of the SAF-N and SAF-M fronts. Mean locations of the fronts

are shown with dotted (SAF-N) and dashed (SAF-M) lines. The location of specific eddies is indicated as A1-A4 for anticyclonic eddies and C1 for a cyclonic eddy.

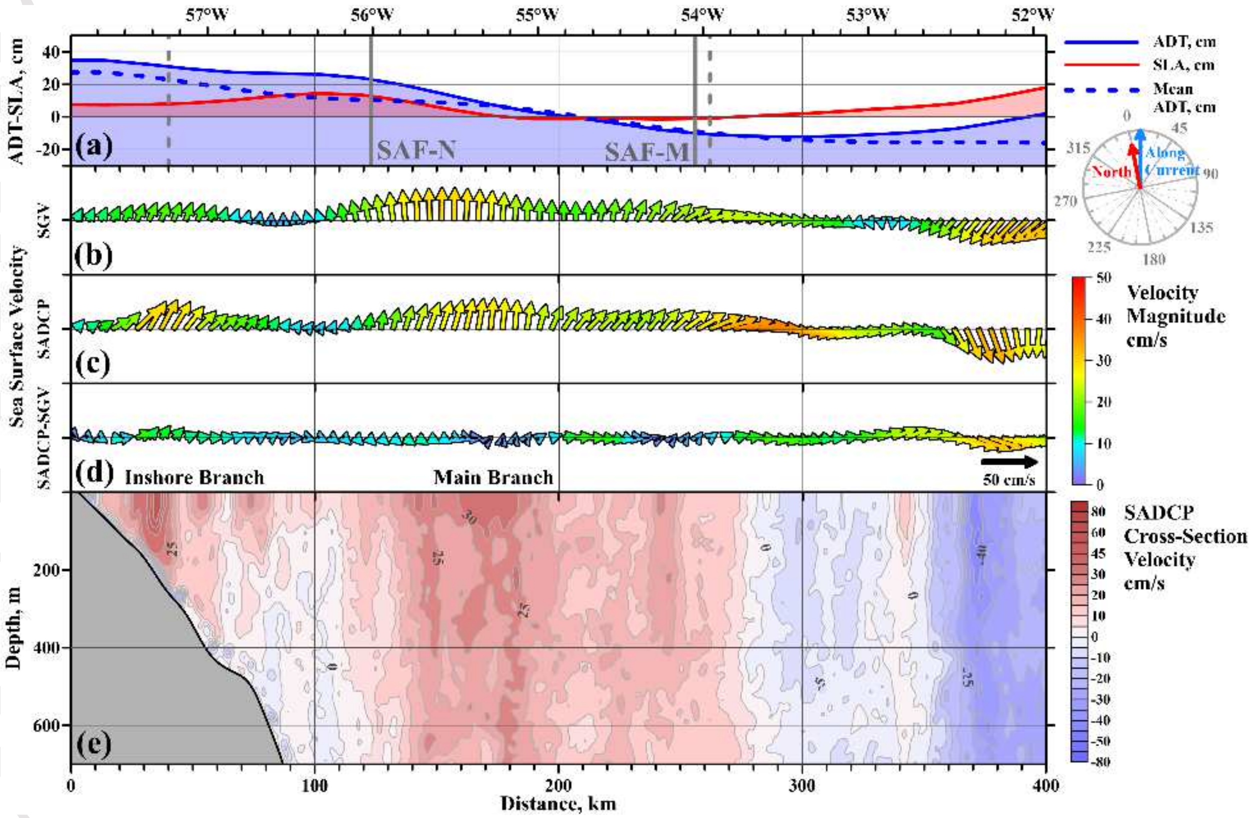

Figure 8. Transect 3, occupied over the Falkland/Malvinas Plateau on October 21-25, 2017 (Crossing 8; see Table 1 and Figure 2 for location). Top panel (a): altimetry data at the time of measurements: Absolute Dynamic Topography (ADT, solid blue line), Sea Level Anomaly (SLA, solid red line), and time mean ADT (dashed blue line). Panel (b): satellite-derived sea surface geostrophic velocities (SGV) along the SADCP transect. Panel (c): sea surface velocities based on the SADCP data. Panel (d): difference between measured and altimetry-derived velocities. The true north and along-slope directions are shown to the right of panels (a) and (b). Bottom panel (e): along-slope SADCP velocities across the MC. The main and northern branches of the Subantarctic Front are shown with dashed gray lines based on the isolines of mean sea surface height of -10 cm and 23 cm according to (Barre et al., 2011). The synoptic location of the same isolines is shown with vertical solid gray lines.

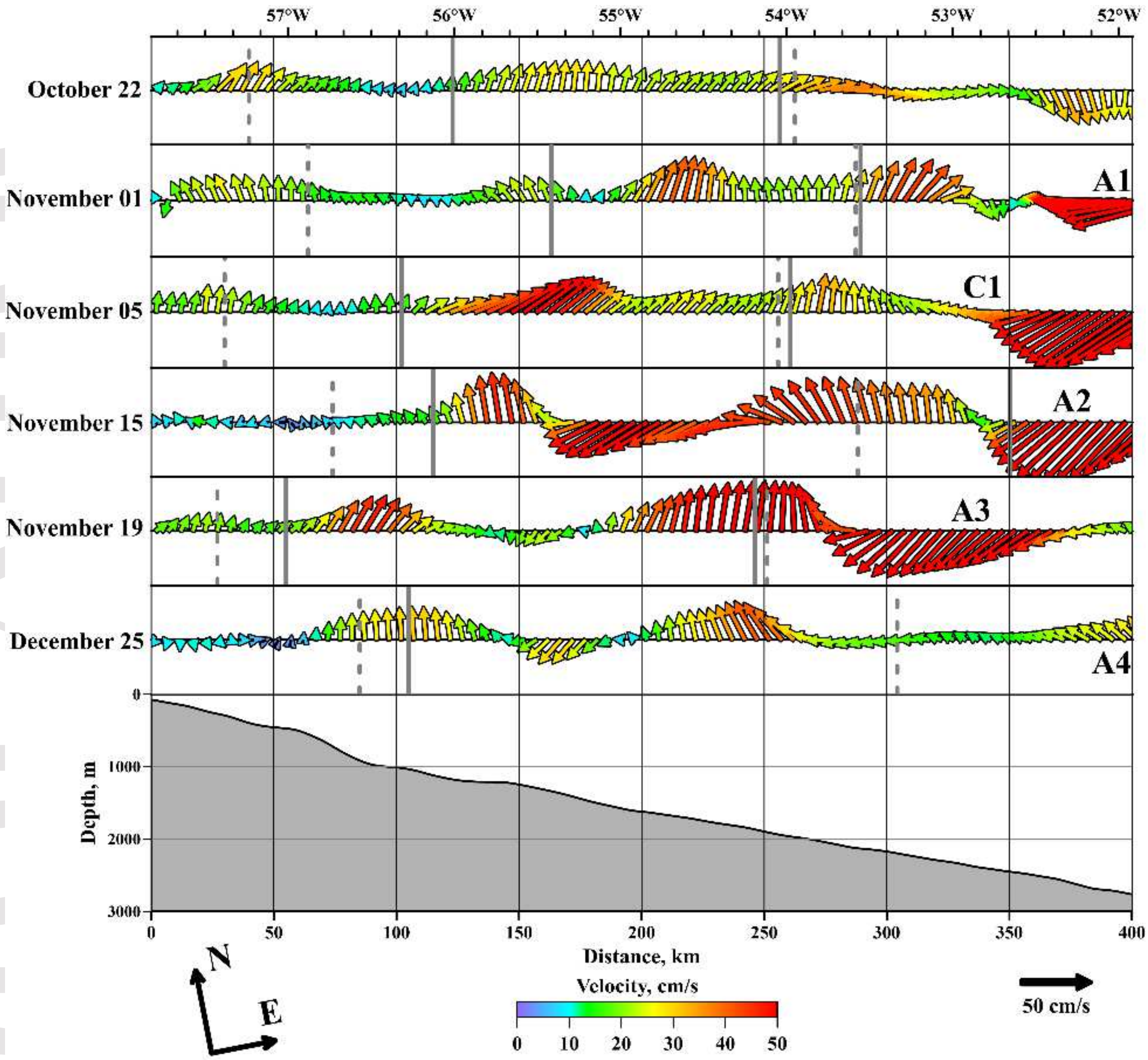

Figure 9. Sea surface velocities over the Falkland/Malvinas Plateau along Transect 3 based on SADCP data collected during six crossings of the MC in October-December 2017. Corresponding synoptic maps of altimetry-derived velocities on the same dates are given in Figure 7. Solid gray lines indicate the synoptic location of the SAF-N and SAF-M fronts; dashed lines indicate the mean locations of these fronts. Note that transect locations do not exactly match, leading to the observed displacement of time-averaged front locations. The lower panel shows the mean bathymetry based on the GEBCO version 2019 data interpolated over the section. In each crossing the locations of specific eddies indicated in Figure 7 are shown (A1-A4 and C1).

Further insight on the time variability of the velocity field over the Falkland/Malvinas Plateau is provided by the comparison of the SADCP derived surface velocities observed during each occupation (Figure 9). The shallow Falkland/Malvinas Plateau is a hotspot for dissipation of the eddy kinetic energy (EKE) spreading from the Drake Passage, which decreases from > 600 cm^2/s^2 to ~ 300 cm^2/s^2 across the North Scotia Arc (Artana et al., 2016). Maximum velocities and their location relative to the shore vary significantly. As pointed out above, in some crossings, the inshore or main branches split into two separate jets. Bands of opposite flow (directed southwestward) are observed at all crossings; they are especially strong in the area east of the main branch where flow speeds are usually as high as in the main branch (up to 72 cm/s). The altimetry confirms the presence of this opposite flow at the sea surface. At some crossings, the inshore jet shifts significantly offshore. For example, measurements performed on November 15, 2017 show that the center of the inshore branch is located almost 150 km from the coast.

The flow structure along Transect 4 is similar to the structure along Transect 3 (Figures 10a and 11). The inshore branch is characterized by the near-surface maximum velocities of 55 cm/s located over the 250-m isobath; the main branch, with velocities up to 45 cm/s is located over the 1500 m isobath. The speeds are approximately 10 cm/s higher than those observed in Transect 3, which is confirmed by direct measurements and satellite altimetry. A cyclonic eddy is observed in the northern part of the transect (centered at a distance of 350 km from the shore in Figure 11, also see Figure 10a); it is revealed both in the altimetry and direct velocity observations. Our route crossed almost the center of this cyclonic eddy. Two velocity maxima were found in the main branch of the MC, which are located one above the other: one maximum is observed near the sea surface (45 cm/s) and the other one at 400 m depth (41 cm/s). The sharp northern boundary of the current (at about 300 km from shore) is due to the presence of the previously mentioned eddy, which drives a relatively intense southwestward counterflow (27 cm/s) just north (offshore) of the main MC branch. The inshore and main branches are separated by a band of low velocities approximately 100 km wide and some filaments of weak reversing currents (less than 10-15 cm/s) which extend to the ocean bottom. A separate high-velocity flow is observed at 300 km from the shore at a depth of 550 m. The maximum velocity within this core is 31 cm/s; the flow is directed along the slope (as the entire main branch, to the west and northwest, see Supporting Information, Figure S27). The distance between this subsurface core and the slope is ~100 km. It should be noted that the data from the deepest levels are generally less accurate than those from the surface layers due to weaker reflected signal.

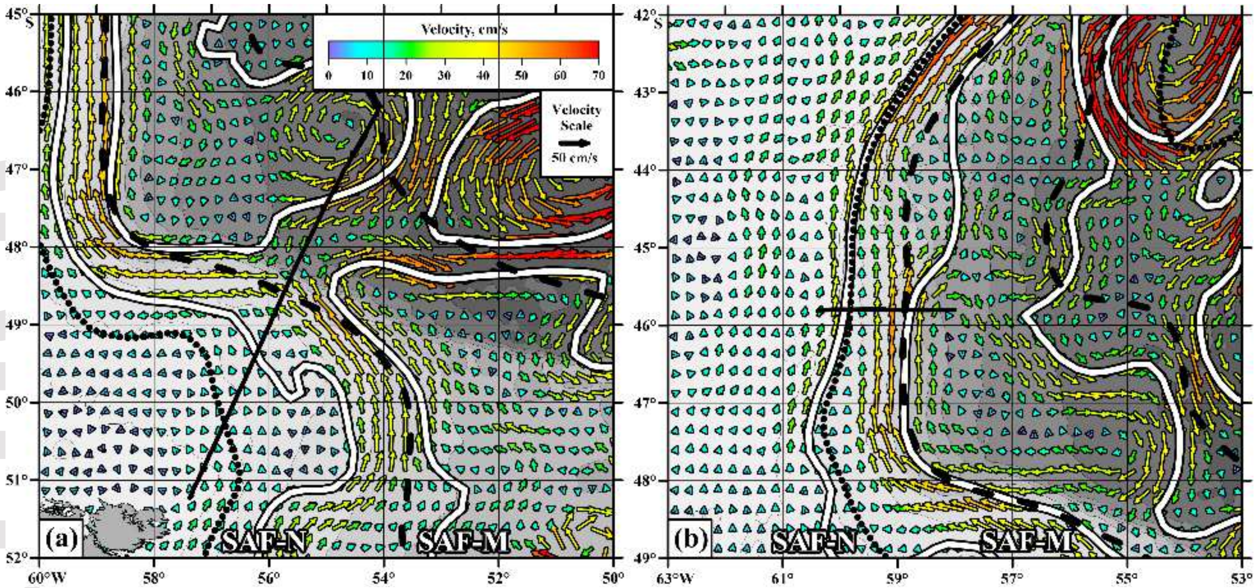

Figure 10. Altimetry-derived sea surface geostrophic circulation in the Argentine Basin on October 19, 2017 (a) and January 12, 2020 (b). The dates correspond to crossings 14 and 16 (see Table 1 for additional information). Black lines denote ship routes along Transects 4 (a) and 5 (b); white lines are synoptic locations of the SAF-N and SAF-M fronts. Mean locations of the fronts are shown with dotted (SAF-N) and dashed (SAF-M) lines.

3.3. The Malvinas Current along the western margin of the Argentine Basin

Satellite altimetry fields suggest that the position of the MC is very stable in the Argentine Basin compared to the Falkland/Malvinas Plateau, probably steered by the sharp bottom slope, and the current velocities remain relatively high up to the Confluence zone. Two zonal crossings were performed approximately along 46°S (Figures 10b and 12).

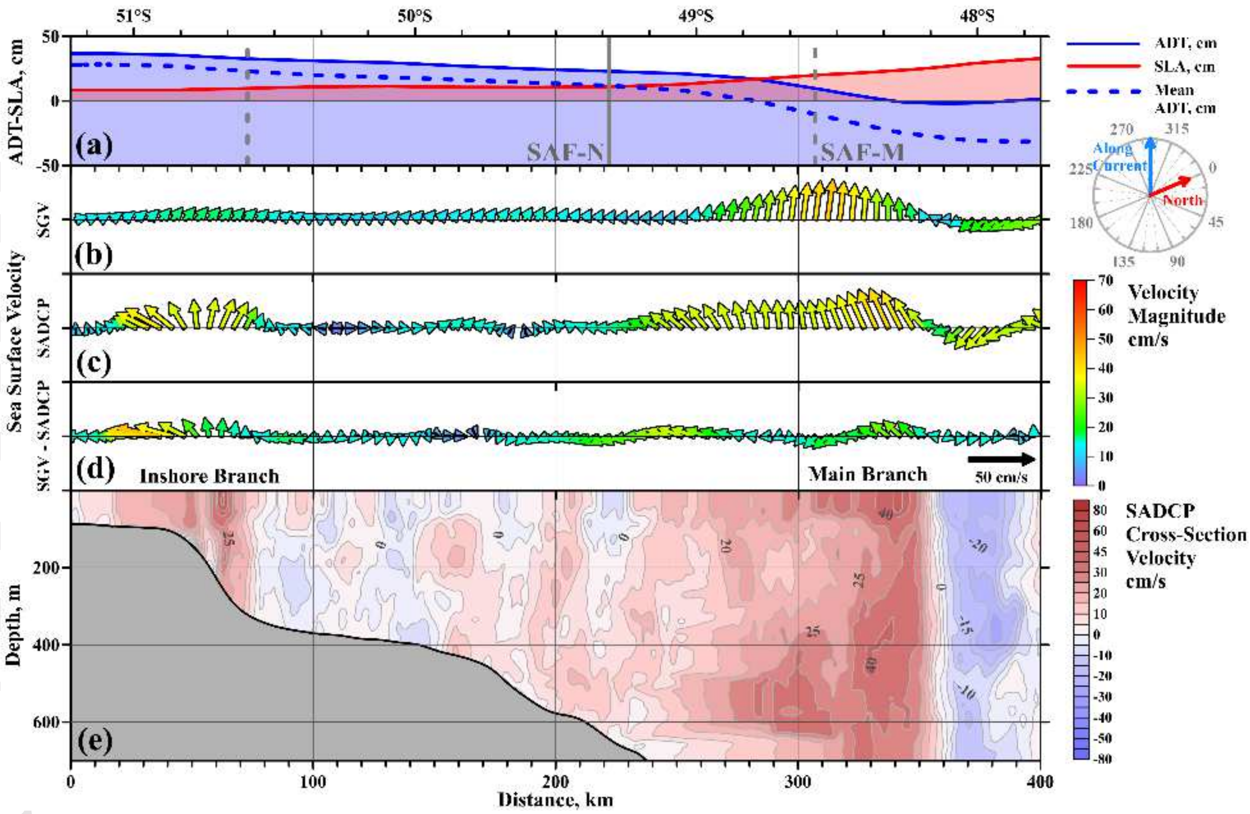

Figure 11. Transect 4, occupied over the Falkland/Malvinas Plateau on October 16-21, 2017 (Crossing 14; see Table 1 and Figure 2 for location). Top panel (a): altimetry data at the time of measurements: Absolute Dynamic Topography (ADT, solid blue line), Sea Level Anomaly (SLA, solid red line), and time mean ADT (dashed blue line). Panel (b): satellite-derived sea surface geostrophic velocities (SGV) along the SADCP transect. Panel (c): sea surface velocities based on the SADCP data. Panel (d): difference between measured and altimetry-derived velocities. The true north and along-slope directions are shown to the right of panels (b), (c), (d). Bottom panel (e): along-slope SADCP velocities across the MC. The main and northern branches of the Subantarctic Front are shown with dashed gray lines based on the isolines of mean sea surface height of -10 cm and 23 cm according to (Barre et al., 2011). The synoptic location of the same isolines is shown with vertical solid gray lines.

Two pronounced current jets are clearly observed along this section; the inshore branch (maximum velocity is 56 cm/s) is observed over the 300 m isobath and the main branch (95 cm/s) is over the 1500-m isobath. The widths of these maximum velocity jets are 4.0 km and 2.7 km for the inner and main cores, respectively; while mean velocities over each branch are 26 cm/s and 39 cm/s. The fastest part of the current is located at or near the sea surface (in the upper 50 m). In the main branch, the velocity decreases almost by half at a depth of 600 meters. The mean vertical shears of the MC are lower at this crossing in comparison with upstream transects: the values of the shear do not exceed 1*10^{-3} s^{-1} and 3*10^{-3} s^{-1} for the inshore and main branches, respectively. The widths of the inshore and main branches are 50 and 150 km, respectively. Satellite-derived geostrophic velocities confirm the two-jet structure of the MC near 46°S (Figure 10b). Based on the altimetry, these two branches appear to merge north of 44°S. Two crossings of the current along this transect show similar velocity structures. Though crossing 15 (Table 1) occupied in November 2016 did not reach the outer shelf, it shows the inshore and main branches of the MC with maximum velocities of 65 and 71 cm/s, respectively (Figure S11). These two sections across the inshore jet reveal variable velocity of the coastal branch, which may be associated with the presence of recently reported trapped waves in the region (Poli et al., 2020). The relatively low sea level anomalies observed in the main part of the current (red line in Figure 12a) are consistent with the low variability characteristic of this region; though intense eddies are usually observed east ~ 58°W (i.e., further offshore from transect 5, e.g., Artana et al., 2018b).

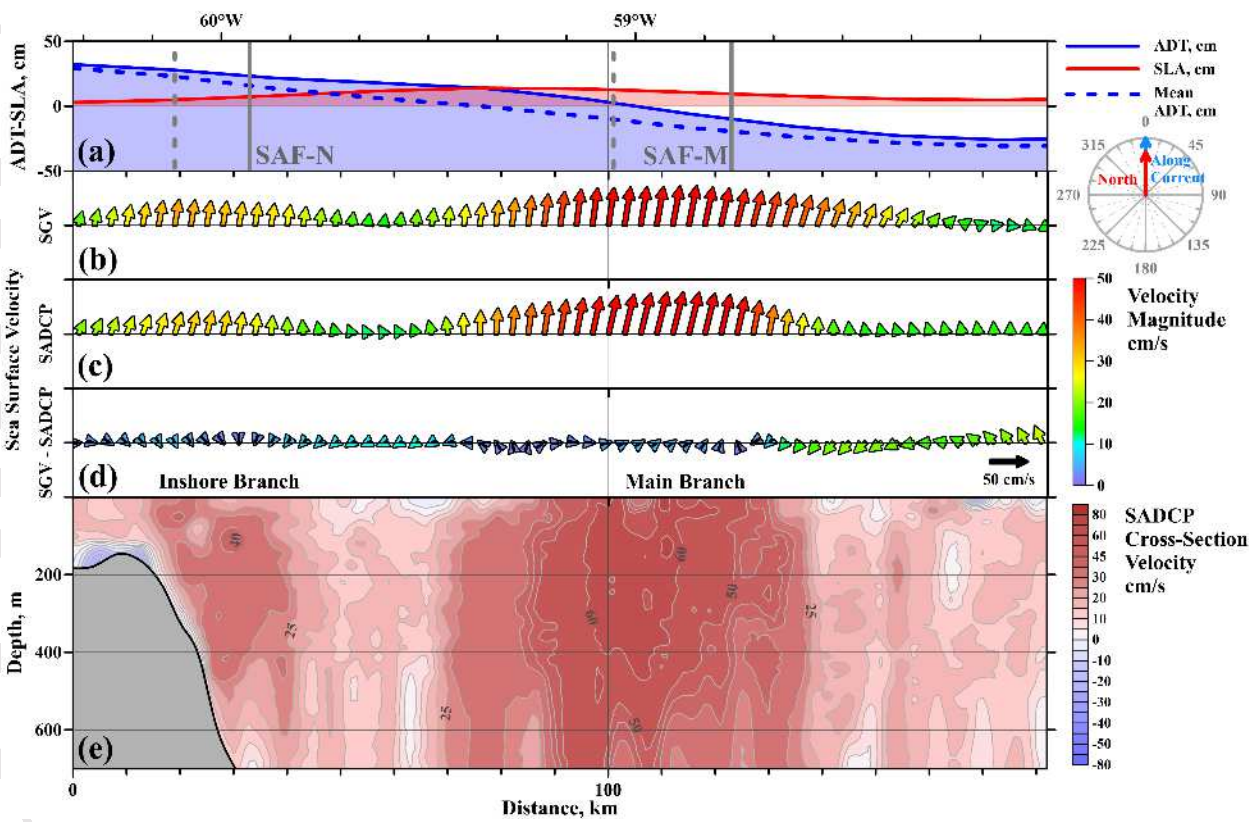

Figure 12. Transect 5, occupied in the western Argentine Basin on January 12-13, 2020 (Crossing 16; see Table 1 and Figure 2 for location). Top panel (a): altimetry data at the time of measurements: Absolute Dynamic Topography (ADT, solid blue line), Sea Level Anomaly (SLA, solid red line), and time mean ADT (dashed blue line). Panel (b): satellite-derived sea surface geostrophic velocities (SGV) along the SADCP transect. Panel (c): sea surface velocities based on the SADCP data. Panel (d): difference between measured and altimetry-derived velocities. The

true north and along-slope directions are shown to the right of panels (a) and (b). Bottom panel (e): along-slope SADCP velocities across the MC. The main and northern branches of the Subantarctic Front are shown with dashed gray lines based on the isolines of mean sea surface height of -10 cm and 23 cm according to (Barre et al., 2011). The synoptic location of the same isolines is shown with vertical solid gray lines.

4. Volume transport variations along the MC path.

There are several estimates of volume transport of the MC at different locations, different depth ranges, and application of different methods. In the following subsections, we overview the existing transport estimates (4.1) and estimate the transports in the upper 700 m based on our SADCP data (4.2).

4.1. Existing estimates of the MC transport

The MC volume transports reported in the literature vary in a wide range (Table 2). The first MC transport estimates were based on geostrophic calculations (Gordon & Greengrove, 1986; Maamaatuaiahutapu et al., 1998). Calculations of geostrophic velocities from hydrographic data require the choice of a reference level. The problem of this choice for the MC is in its strong barotropic structure; the current extends to the bottom and causes high uncertainties in the volume transport based on baroclinic geostrophic calculations derived from hydrographic observations. This emphasizes the value of directly measured velocities. In addition, the sharp bottom slope precludes estimating the baroclinic shear in portions of the water column below the deepest observation of the shallowest station of each pair (i.e., the well-known bottom triangle problem). The combination of hydrographic observations with satellite altimetry data and adjusted to direct velocity measurements gives about 50 Sv at 45°S (Saunders & King, 1995), 41.5±12.5 Sv at 40 – 41°S (Vivier & Provost, 1999b), and 37.1 ± 2.6 Sv at 41ºS (Artana et al., 2018a, and references therein). These relatively high transports indicate the strong contribution of the barotropic flow, which cannot be determined only based on geostrophic calculations from hydrographic data.

Table 2. Volume transports of the MC at different transects based on the literature data

Location of the transect	Depth range, m	Method	Transport, Sv	Source

46°S	Upper 2000 m	Geostrophic	70	(Peterson, 1992)
46°S	Upper 1400 m	Geostrophic	10	(Gordon & Greengrove, 1986)
46°S	Above 800-dbar isobaric surface	Geostrophic	3.4 – 12.4	(Remeslo et al., 2004)
46°S	Upper 600 m	SADCP	20.7	(Morozov et al., 2016)
46°S	Surface to bottom	LADCP	30.9	(Morozov et al., 2016)
near 45°S	Surface to bottom	Geostrophic adjusted with direct current observations	50	(Saunders & King, 1995)
45°S	30–400 m	SADCP	20.8	(Piola et al., 2013)
42°S	Upper 1400 m	Geostrophic	10	(Gordon & Greengrove, 1986)
40 – 41°S	Surface to bottom	Satellite altimetry with direct current observations	41.5±12.5	(Vivier & Provost, 1999b)
40 – 41°S	Surface to bottom	Satellite altimetry with direct current observations	35±7.5 Sv	(Spadone & Provost, 2009)
40 – 41°S	Surface to bottom	Current meters deployed on moorings	37.1	(Artana et al., 2018a)
Part of the current in the Argentine Basin	Surface to bottom	Numerical simulations	Northward decrease from 70 to 54 Sv	(Fetter & Matano, 2008)
40-41°S	Surface to bottom	Numerical simulations	40	Combes & Matano (2014)

The variability of the baroclinic volume transport is discussed in (Remeslo et al., 2004) on the basis of a series of 140 hydrographic sections occupied along 46°S; these transports vary from 12.4 to 3.4 Sv in the upper layer of the current (relative to and above 800-dbar). Moorings deployed at 40 – 41°S show significant variability of the MC transports with a mean value of 37.1 Sv and a standard deviation of 6.6 Sv (Artana et al., 2018a). Estimates based on the direct SADCP measurements performed at 46°S give 20.7 Sv in the upper 600 m and 30.9 Sv over the same section with measurements from the sea surface to the bottom performed by LADCP (Morozov et al., 2016). In this work, the estimates were made separately in the narrow (~20-km) bands associated with the inshore and offshore branches (3.2 and 4.0 Sv above 400 m, respectively). In the following section, we present separate estimates for the two main branches of the MC.

4.2. Calculations of the transport based on the SADCP data

We calculate the transport of the MC in the upper 700 m for each crossing of the current in the Argentine Basin and over the Falkland/Malvinas Plateau. Mean values of these transports are given in Table 3 for each transect; the data for each individual crossing are presented in Supporting Information (Table S1). As we have observed two distinct branches at every transect, we estimated the transport individually for each branch and then computed the total transport of the MC. The transport of the main branch for Transects 1 and 2 is not presented because in this region the current is part of the ACC upstream from the bifurcation west and east of the Burdwood Bank (Figure 5) making it difficult to determine what fraction of the flow veers northward (i.e., along the MC path) and eastward following the ACC. In addition, as noted earlier, meandering of the SAF and PF preclude a clear distinction of the transport associated with the SAF. We also list the maximum along-current velocities for each branch in Table 3. Standard deviation of the velocity maximum value is also shown in Table 3. It should be noted that our estimates of maximum velocities at transects 1 and 2 can be associated with the merged Subantarctic and Polar fronts depending on their actual position during the occupation of each transect. To estimate the volume transport, we interpolated these data to a regular grid 1 km wide and 8 m thick and integrated the transport between the sea surface and 700 m or ocean bottom in shallower areas. In addition, we extrapolated these data to the sea surface using the nearest neighbor method. The velocities extrapolated to the surface are quite reliable for the transport calculations of the whole current due to the barotropic structure of the flow and relatively small thickness of the unsampled near-surface layer (18-22 m). The velocity data across each section were integrated over the area of each branch; we defined the boundary between the branches based on the minimum value of the along-flow velocity at the sea surface between the cores of the two MC branches. We present the exact limits of the transport calculations in Table S2 of Supporting Information. Thus, subtraction of tidal velocities is important for more precise transport calculations. We integrated both positive and negative components of cross-section velocities and then calculated their sum for the total estimate of the transport through the transect (Table 3 and Table S1).

The inshore branch transports vary from 2.4 to 6.3 Sv, which represents 10-15% of the total MC transport (Table 3). The transport of the main branch varies downstream along the MC path in the Argentine Basin from 23.4 to 25.4 Sv. Variations of the inshore branch transport are higher; the transport varies between 2.4 and 6.3 Sv at different locations. The minimum transport is observed at Transect 4, while transports at Transects 3 and 5 are significantly higher. The total transport of both MC branches based on our SADCP measurements reaches almost 30 Sv at 46°S. The transport increase between Transects 4 and 5 may be due to a recirculation cell within the cyclonic loop of the MC in the western Argentine Basin (e.g., Peterson, 1992). However, the 700 m integration limit imposed by the SADCP observations are probably too shallow and preclude fully explaining the along-path transport variations of the MC. Moreover, Transect 4 was occupied only once and the transects were occupied at different times. Thus, a detailed analysis of the transport variations along the MC path requires additional data. Though the transport have been estimated at different locations and on different dates, they are based on high cross-flow resolution observations and can therefore be helpful for validation of transport estimates based on other observational methods and numerical simulations.

Table 3. The volume transports and maximum velocities of both MC branches at different transects across the current. Numbers of the transects are specified in Figure 2 and Table 1.

Transect Number	Inshore Branch						Main Branch						Total transport, Sv
	Mean Transport, Sv	Standard deviation of transport, Sv	Maximum Velocity, cm/s	Standard deviation of V, cm/s	Depth of the velocity maximum, m	Maximum of altimetry derived velocity, cm/	Mean Transport, Sv	Standard deviation of transport, Sv	Maximum Velocity, cm/s	Standard deviation of V, m/s	Depth of the velocity maximum, m	Maximum of altimetry derived velocity, cm/	
1	4.2±1.1	2.8	84	17	0 – 95	36	-	-	94	16	0 – 250	78	-
2	6.3±1.4	-	51	-	0	21	-	-	88	-	250	71	-
3	6.0±1.0	3.3	58	14	0 – 115	17	23.4±1.5	6.8	63	12	0 – 250	30	29.4±2.5
4	2.4±0.7	-	59	-	0	13	21.3±2.5	-	57	-	0	31	23.7±3.2

5	4.4± 0.4	1.0	61	6	100 – 110	35	25.4 ±3.0	1.1	83	17	130 – 150	53	29.8 ±3.4

5. Summary and Conclusions

Despite the fact that the spatial structure of the MC has been addressed in numerous studies, direct measurements of the velocity field remain quite rare. In this work, we analyzed a set of recent observations performed along a series of cross-flow transects occupied in 2016 – 2020, focused on the spatial distribution of the current velocities. Further studies are needed to better understand the dynamics of this region. As altimetry-derived sea surface circulation is known to reproduce the main circulation patterns at time scales longer than about 20 days, these data can be used to investigate the spatial and temporal variability of the surface manifestation of the MC branches. There is a good overall agreement between altimetry and direct current observations and altimetry provides helpful information on the regional circulation. Temporal variability of the volume transports can also be studied by the altimetry data, but high horizontal resolution subsurface observations may be required to properly assess the impact of the ubiquitous high velocity cores revealed by the SADCP data on the MC transport. The first results of the analysis performed in this work are listed below:

1. High velocities are observed along the current pathway from the Drake Passage up to 46° S. Though the overall vertical structure of the MC is characterized by low to moderate vertical shear, as reported in previous studies, the direct SADCP measurements indicate that the highest velocities are observed in the upper layer with a thickness of 200-400 m depending on the transect. The vertical shears of the inshore and main MC branches reach $3*10^{-3}$ s^{-1} and $1*10^{-3}$ s^{-1}, respectively; with higher shears observed in the inshore branch. At some sections, the maximum speed is found at the sea surface; at others, it can be located as deep as 200 – 400 m.

2. The main feature of the velocity structure of the current revealed by the SADCP observations is the existence of two MC branches. The branches are observed at all transects occupied along the pathway of the northern ACC and MC up to 46°S. Most transects reveal a band

of opposite flow or significantly lower along-slope velocities located between the two MC branches. These low or opposite velocity bands are 50-200 km wide and are observed in both SADCP and altimetry data. The inshore current branch presents relatively stable velocities along the current pathway, reaching up to 60 – 80 cm/s and closely follows the 200 – 300 m isobaths. The vertical and horizontal shears in the inshore branch are large in comparison with the main branch. As a result, the total transport of this branch is rather small. The velocity of the main branch is more variable along the current pathway exceeding 90 cm/s in the northern Drake Passage and 70 cm/s at 46°S in the western Argentine Basin, while the velocity decreases over the Malvinas/Falkland Plateau.

3. The inshore and offshore branches diverge sharply southwest of the Burdwood Bank. The shallow passage between Estados Island and the Burdwood Bank allows only the shallow branch to flow northward and follow the upper continental slope, thus marking the initiation of the inner MC branch. In contrast, the main branch veers northward east of the Burdwood Bank, where the mean flow bifurcates, part flowing northward and feeding the main MC branch and part of the flow continuing eastward as part of the ACC. At this point, these two MC branches are more than 300 km apart from each other.

4. Relatively high maximum velocities (51-84 cm/s) are observed along the inshore branch of the MC. In contrast, in the main branch relatively high maximum velocities are observed in the Drake Passage and western Scotia Sea (88-94 cm/s) and in the Argentine Basin (83 cm/s), but the velocities decrease to 57 – 63 cm/s over the western Falkland/Malvinas Plateau. These spatial changes in sea surface velocities are confirmed by satellite altimetry data.

5. Calculations of the volume transports based on the direct SADCP measurements in the waters shallower than 700 m vary from 2.4 to 6.3 Sv in the inshore branch and from 21.3 to 25.4 Sv in the main branch.

Acknowledgements

This work was supported by the State Task of Russia 0128-2021-002 (ship expenses), the Russian Science Foundation Grant 21-77-20004 (field studies) and Russian Foundation for Basic Research grants 19-57-60001 (calculation of the sea surface velocities), 18-05-00283 (measurements of the ACC in the Drake Passage), and 18-05-00194 (analysis of the field and satellite data). ARP acknowledges the support of grant D3347/14 from CONICET (Argentina) and the Inter-American Institute for Global Change Research grant CRN3070. We thank the editor and two reviewers for providing comments that helped improving the final version of this manuscript. All experimental data used in the publication are available in open access through Pangaea (https://doi.pangaea.de/10.1594/PANGAEA.925224). The satellite altimetry data are available at Copernicus Marine Environment Monitoring Service (CMEMS; http://marine.copernicus.eu/).

References

1. Arhan, M., Naveira Garabato, A. C., Heywood, K. J., & Stevens, D. P. (2002). The Antarctic Circumpolar Current between the Falkland Islands and South Georgia. Journal of Physical Oceanography, 32(6), 1914-1931. https://doi.org/10.1175/1520-0485(2002)032<1914:TACCBT>2.0.CO;2
2. Artana, C., Ferrari, R., Bricaud, C., Lellouche, J. M., Garric, G., Sennéchael, N., ... & Provost, C. (2019b). Twenty-five years of Mercator ocean reanalysis GLORYS12 at Drake Passage: velocity assessment and total volume transport. Advances in Space Research. https://doi.org/10.1016/j.asr.2019.11.033
3. Artana, C., Ferrari, R., Koenig, Z., Saraceno, M., Piola, A. R., & Provost, C. (2016). Malvinas Current variability from Argo floats and satellite altimetry. Journal of Geophysical Research: Oceans, 121(7), 4854–4872. https://doi.org/10.1002/2016JC011889
4. Artana, C., Ferrari, R., Koenig, Z., Sennéchael, N., Saraceno, M., Piola, A. R., & Provost, C. (2018a). Malvinas Current volume transport at 41 °S: A 24 yearlong time series consistent with mooring data from 3 decades and satellite altimetry. Journal of Geophysical Research: Oceans, 123(1), 378–398. https://doi.org/10.1002/2017JC013600
5. Artana, C., Lellouche, J. M., Park, Y. H., Garric, G., Koenig, Z., Sennéchael, N. & Provost, C. (2018b). Fronts of the Malvinas Current System: surface and subsurface expressions revealed by satellite altimetry, Argo floats, and Mercator operational model outputs. Journal of Geophysical Research: Oceans, 123(8), 5261–5285. https://doi.org/10.1029/2018JC013887
6. Artana, C., Provost, C., Lellouche, J. M., Rio, M. H., Ferrari, R., & Sennéchael, N. (2019a). The Malvinas current at the confluence with the Brazil current: Inferences from 25 years

of Mercator ocean reanalysis. Journal of Geophysical Research: Oceans, 124(10), 7178-7200. https://doi.org/10.1029/2019JC015289

7. Balech E. (1949) Estudio critico de las corrientes marinas del Litoral Argentino. , Physis 20(57), 159–164.

8. Barré, N., Provost, C., Renault, A., & Sennéchael, N. (2011). Fronts, meanders and eddies in Drake Passage during the ANT-XXIII/3 cruise in January–February 2006: A satellite perspective. Deep Sea Research Part II: Topical Studies in Oceanography, 58(25-26), 2533-2554. https://doi.org/10.1016/j.dsr2.2011.01.003

9. Brennecke W. (1921) Die ozeanographischen Arbeiten der deutschen Antarktischen Expedition 1911-1912. Aus dem Archiv der Deutschen Seewart, 39, 1–216.

10. Chelton, D.B., Schlax, M.G., Witter, D.L. and Richman, J.G. (1990). Geosat altimeter observations of the surface circulation of the Southern Ocean. Journal of Geophysical Research: Oceans, 95(C10), pp.17877-17903.

11. Chereskin, T. K., & Harris, C. L. (1997). Shipboard acoustic Doppler current profiling during the WOCE Indian Ocean expedition: I10. Scripps Institution of Oceanography, University of California, San Diego. 137pp.

12. Combes, V., & Matano R. P. (2014). A two-way nested simulation of the oceanic circulation in the Southwestern Atlantic, J. Geophys. Res. Oceans, 119, 731–756. https://doi.org/10.1002/2013JC009498

13. Combes, V., & Matano, R. P. (2018). The Patagonian shelf circulation: Drivers and variability. Progress in Oceanography, 167, 24-43. https://doi.org/10.1016/j.pocean.2018.07.003

14. Cunningham, S., S. Alderson, B. King, & M. Brandon (2003). Transport and variability of the Antarctic Circumpolar Current in Drake Passage. J. Geophys. Res., 108(C5), 8084. https://doi.org/10.1029/2001JC001147.

15. Davis, R. E., Regier, L. A., Dufour, J., & Webb, D. C. (1992). The autonomous Lagrangian circulation explorer (ALACE). Journal of atmospheric and oceanic technology, 9(3), 264–285. https://doi.org/10.1175/1520-0426(1992)009<0264:TALCE>2.0.CO;2

16. Donohue, K. A., K. L. Tracey, D. R. Watts, M. P. Chidichimo, & T. K. Chereskin (2016). Mean Antarctic Circumpolar Current transport measured in Drake Passage. Geophys. Res. Lett., 43, 11,760–11,767. https://doi.org/10.1002/2016GL070319.

17. de Moraes Rudorff, N., Frouin, R., Kampel, M., Goyens, C., Meriaux, X., Schieber, B., & Mitchell, B. G. (2014). Ocean-color radiometry across the Southern Atlantic and Southeastern Pacific: Accuracy and remote sensing implications. Remote Sensing of Environment, 149, 13–32. https://doi.org/10.1016/j.rse.2014.03.029
18. Deacon, G. E. R. (1937). The hydrology of the Southern Ocean. Discovery Reports. 15, 1–124.
19. Egbert, G. D., & Erofeeva, S. Y. (2002). Efficient inverse modeling of barotropic ocean tides. Journal of Atmospheric and Oceanic technology, 19(2), 183-204. https://doi.org/10.1175/1520-0426(2002)019<0183:EIMOBO>2.0.CO;2.
20. Ferrari, R., Provost, C., Renault, A., Sennéchael, N., Barré, N., Park, Y. H., & Lee, J. H. (2012). Circulation in Drake Passage revisited using new current time series and satellite altimetry: 1. The Yaghan Basin. Journal of Geophysical Research: Oceans,117(C12). https://doi.org/10.1029/2012JC008264
21. Ferrari, R., Artana, C., Saraceno, M., Piola, A. R., & Provost, C. (2017). Satellite altimetry and current-meter velocities in the Malvinas Current at 41°S: Comparisons and modes of variations. Journal of Geophysical Research: Oceans, 122, 9572–9590. https://doi.org/10.1002/2017JC013340
22. Fetter, A. F., & Matano, R. P. (2008). On the origins of the variability of the Malvinas Current in a global, eddy-permitting numerical simulation. Journal of Geophysical Research: Oceans, 113(C11). https://doi.org/10.1029/2008JC004875
23. Firing, Y. L., Chereskin, T. K., & Mazloff, M. R. (2011). Vertical structure and transport of the Antarctic Circumpolar Current in Drake Passage from direct velocity observations. Journal of Geophysical Research: Oceans, 116(C8). https://doi.org/10.1029/2011JC006999
24. Firing, E., Hummon, J. M., & Chereskin, T. K. (2012). Improving the quality and accessibility of current profile measurements in the Southern Ocean. Oceanography, 25(3), 164-165 https://doi.org/10.5670/oceanog.2012.91
25. Franco, B. C., Piola, A. R., Rivas, A. L., Baldoni, A., & Pisoni, J. P. (2008). Multiple thermal fronts near the Patagonian shelf break. Geophysical Research Letters, 35(2). https://doi.org/10.1029/2007GL032066

26. Gordon, A. L., & Greengrove, C. L. (1986). Geostrophic circulation of the Brazil-Falkland confluence. Deep Sea Research Part A. Oceanographic Research Papers, 33(5), 573–585. doi:10.1016/0198-0149(86)90054-3

27. Guihou, K., Piola, A. R., Palma, E. D., & Chidichimo, M. P. (2020) Dynamical Connections between Large Marine Ecosystems of Austral South America based on numerical simulations. Ocean Science, 6, 271–290, doi: 10.5194/os-16-271-2020.

28. Kim, Y.S., & Orsi, A.H. (2014). On the variability of Antarctic Circumpolar Current fronts inferred from 1992–2011 altimetry. Journal of Physical Oceanography, 44(12), 3054-3071. https://doi.org/10.1175/JPO-D-13-0217.1

29. Legeckis, R., & Gordon, A. L. (1982). Satellite observations of the Brazil and Falkland Currents-1975 to 1976 and 1978. Deep Sea Res., 29(3), 375–401, https://doi.org/10.1016/0198-0149(82)90101-7

30. Lenn, Y. D., Chereskin, T. K. (2009). Observations of Ekman currents in the Southern Ocean. Journal of Physical Oceanography, 39(3), 768-779. https://doi.org/10.1175/2008JPO3943.1

31. Maamaatuaiahutapu, K., Garçon, V., Provost, C., & Mercier, H. (1998). Transports of the Brazil and Malvinas Currents at their Confluence. Journal of Marine Research, 56(2), 417–438. https://doi.org/10.1357/002224098321822366

32. Magalhaes, J. M., & da Silva, J. C. (2017). Internal Waves Along the Malvinas Current Evidence of transcritical generation in satellite imagery. Oceanography, 30(3), 110–119. https://doi.org/10.5670/oceanog.2017.319.

33. Meredith, M. P., Woodworth, P. L., Chereskin, T. K., Marshall, D. P., Allison, L. C., Bigg, G. R., ... & Hogg, A. M. (2011). Sustained monitoring of the Southern Ocean at Drake Passage: Past achievements and future priorities. Reviews of Geophysics, 49(4). https://doi.org/10.1029/2010RG000348

34. Morozov, E. G., Tarakanov, R. Y., Demidova, T. A., Frey, D. I., Makarenko, N. I., Remeslo, A. V., & Gritsenko, A. M. (2016). Velocity and transport of the Falkland Current at 46°S, Russ. J. Earth. Sci., 16(6), ES6005. doi:10.2205/2016ES000588.

35. Painter, S. C., Poulton, A. J., Allen, J. T., Pidcock, R., & Balch, W. M. (2010). The COPAS-08 expedition to the Patagonian Shelf: Physical and environmental conditions

during the 2008 coccolithophore bloom, Cont. Shelf Res., 30(18), 1907–1923. https://doi.org/10.1016/j.csr.2010.08.013

36. Pérez-Hernández, M. D., Hernández-Guerra, A., Comas-Rodríguez, I., Benítez-Barrios, V. M., Fraile-Nuez, E., Pelegrí, J. L., & Naveira Garabato, A. C. (2017). Differences between 1999 and 2010 across the Falkland Plateau: fronts and water masses. Ocean Science, 13(4), 577-587. https://doi.org/10.5194/os-13-577-2017
37. Peterson, R. G. (1992). The boundary currents in the western Argentine Basin. Deep Sea Research Part A. Oceanographic Research Papers, 39(3–4), 623–644. https://doi.org/10.1016/0198-0149(92)90092-8
38. Peterson, R. G., & Whitworth III, T. (1989). The Subantarctic and Polar Fronts in relation to deep water masses through the southwestern Atlantic. Journal of Geophysical Research: Oceans, 94(C8), 10817-10838. https://doi.org/10.1029/JC094iC08p10817
39. Peterson, R. G., Johnson, C. S., Krauß, W., & Davis, R. E. (1996) Lagrangian Measurements in the Malvinas Current. In: The South Atlantic. (pp. 239–247) Edited by G. Weffer, W. H. Berger, G. Siedler and D. J. Webb. Springer, Berlin, Heidelberg. https://doi.org/10.1007/978-3-642-80353-6_12
40. Piola, A. R., & Gordon, A. L. (1989). Intermediate waters in the southwest South Atlantic. Deep-Sea Res, 36(1), 1-16. https://doi.org/10.1016/0198-0149(89)90015-0
41. Piola, A. R., & Matano, R. P. (2019). Ocean Currents: Atlantic Western Boundary—Brazil Current/Falkland (Malvinas) Current. Earth Systems and Environmental Sciences, 1-7
42. Piola, A. R., Franco, B. C., Palma, E. D., & Saraceno, M. (2013). Multiple jets in the Malvinas Current. Journal of Geophysical Research: Oceans, 118(4), 2107–2117. https://doi.org/10.1002/jgrc.20170
43. Poli, L., Artana, C., Provost, C., Sirven, J., Sennéchael, N., Cuypers, Y., Lellouche J.-M. (2020). Anatomy of subinertial waves along the Patagonian shelf break in a 1/12° global operational model. Journal of Geophysical Research: Oceans, 125 (12) https://doi.org/10.1029/2020JC016549
44. Provost, C., Garcon, V., & Medina Falcon, L. (1996). Hydrographic conditions in the surface layers over the slope-open ocean transition area near the Brazil-Falkland Confluence during Austral summer 1990. Continental Shelf Research, 16(2), 215–235. https://doi.org/10.1016/0278-4343(95)00006-M

45. Pujol, M. I., Faugère, Y., Taburet, G., Dupuy, S., Pelloquin, C., Ablain, M., & Picot, N. (2016). DUACS DT2014: The new multi-mission altimeter data set reprocessed over 20 years. Ocean Science, 12(5), 1067–1090. https://doi.org/10.5194/os-12-1067-2016
46. Remeslo, A. V., Morozov, E. G., Neiman, V. G., & Chernyshkov, P. P. (2004), Structure and variability of the Falkland Current, Doklady Earth Sciences, 399, 1156–1159.
47. Renault, A., Provost, C., Sennéchael, N., Barré, N., & Kartavtseff, A. (2011). Two full-depth velocity sections in the Drake Passage in 2006—Transport estimates. Deep Sea Research Part II: Topical Studies in Oceanography, 58(25-26), 2572-2591. https://doi.org/10.1016/j.dsr2.2011.01.004
48. Rocha, C. B., Chereskin, T. K., Gille, S. T., & Menemenlis, D. (2016). Mesoscale to submesoscale wavenumber spectra in Drake Passage. Journal of Physical Oceanography, 46(2), 601-620. https://doi.org/10.1175/JPO-D-15-0087.1
49. Saraceno, M., Provost, C., Piola, A. R., Bava, J., & Gagliardini, A. (2004). Brazil Malvinas Frontal System as seen from 9 years of advanced very high resolution radiometer data. Journal of Geophysical Research: Oceans, 109(C5).
50. Saunders, P. M., & King, B. A. (1995). Bottom currents derived from a shipborne ADCP on WOCE cruise A11 in the South Atlantic. Journal of Physical Oceanography, 25(3), 329–347. https://doi.org/10.1175/1520-0485(1995)025<0329:BCDFAS>2.0.CO;2
51. Sokolov, S., Rintoul, S. R. (2009). Circumpolar structure and distribution of the Antarctic Circumpolar Current fronts: 1. Mean circumpolar paths. Journal of Geophysical Research: Oceans, 114(C11). doi:10.1029/2008JC005108.
52. Spadone, A., & Provost, C. (2009). Variations in the Malvinas Current volume transport since October 1992. Journal of Geophysical Research: Oceans, 114(C2). https://doi.org/10.1029/2008JC004882
53. Tarakanov, R. Y. (2018). Influence of the Current Field Non-stationarity and the Non-simultaneity of Hydrographic Measurements on ADCP-based Transport Estimates. In: The Ocean in Motion (pp. 361-396). Springer, Cham. https://doi.org/10.1007/978-3-319-71934-4_23
54. Vivier, F., & Provost, C. (1999a). Volume transport of the Malvinas Current: Can the flow be monitored by TOPEX/POSEIDON? Journal of Geophysical Research: Oceans, 104(C9), 21105-21122. https://doi.org/10.1029/1999JC900056

55. Vivier, F., & Provost, C. (1999b). Direct velocity measurements in the Malvinas Current. Journal of Geophysical Research, 104(C9), 21083–21103. https://doi.org/10.1029/1999JC900163

56. Wessel, P., & Smith, W. H. (1996). A global, self-consistent, hierarchical, high-resolution shoreline database. Journal of Geophysical Research: Solid Earth, 101(B4), 8741-8743. https://doi.org/10.1029/96JB00104

57. Willson, H. R., & Rees, N. W. (2000). Classification of mesoscale features in the Brazil-Falkland Current confluence zone. Progress in Oceanography, 45(3–4), 415–426. https://doi.org/10.1016/S0079-6611(00)00011-2

58. Zyrjanov, V. N., & Severov D.N. (1979). Water circulation in the Falkland-Patagonian region and its seasonal variability. Okeanologiya, 29, 782–790.